

# Orbital Hall effect in crystals: inter-atomic versus intra-atomic contributions

Armando Pezo, Diego García Ovalle, and Aurélien Manchon\*

Aix-Marseille Université, CNRS, CINAfM, Marseille, France.

(Dated: April 4, 2022)

The orbital Hall effect (OHE) designates the generation of a charge-neutral flow of orbital angular momentum transverse to an initial charge current. It is the orbital analog to the spin Hall effect (SHE), but does not require spin-orbit coupling. Using linear response theory and realistic simulations, we show that in crystals OHE possesses two sources: the intra-atomic contribution arising from the gyration of the wave packet around the nucleus and the inter-atomic contribution associated with the gyration of the wave packet within the unit cell. Although both contributions find their origin in the ground states' geometry in momentum space, the inter-atomic OHE is much more sensitive to band structure details than the intra-atomic OHE. As a consequence, the inter-atomic OHE tends to dominate in the vicinity of the gap of narrow-gap semiconductors, whereas the intra-atomic OHE dominates in large-gap semiconductors as well as in multiband metals. These results open perspectives for the realization of efficient sources of orbital angular momentum for electrically-controlled orbitronics devices.

*Introduction* - The need for energy-efficient microelectronic solutions has accelerated the efforts to identify degrees of freedom that could complement or replace the electron's charge to carry and store information. Whereas spintronics, which uses the electron's spin angular momentum (SAM) to transmit and manipulate data, is probably the most mature alternative technology to date [1], other directions have emerged in the past two decades, seeking to exploit magnons in magnetic insulators [2] or the valley degree of freedom in certain low symmetry semiconductors [3]. Under these various paradigms, the charge of the electron is replaced by a quantum degree of freedom (SAM or valley) that survives in the semiclassical limit and may encode the information over two distinct values (spin up/down, valley K/K' etc.). In recent research, the control of the SAM is achieved via spin-orbit coupling, a property that scales with the mass of the elements nucleus. Therefore, most progress is currently achieved using heavy materials such as Pt, W, Bi etc. which are scarce and expensive [4]. The emergent field of valleytronics on the other hand exploits the generation of valley-polarized currents induced by light in optically active materials. Whether the valley degree of freedom could be injected in adjacent materials, transported over long distances and stored remains an active area of research. In this context, the orbital angular momentum (OAM) has started to emerge as a promising degree of freedom that could be generated efficiently and transported over long distances [5, 6].

Equilibrium OAM has been investigated thoroughly over the past decade and was shown to substantially contribute to the overall magnetization in certain classes of time-reversal broken materials, associated with the ground state's Berry curvature [7–9]. In fact, equilibrium OAM necessitates time-reversal symmetry breaking combined with either non-collinear magnetic texture or spin-orbit coupling (hence, heavy metal elements) [10, 11].

Although equilibrium OAM vanishes when time-reversal symmetry is preserved, in the presence of an external electric field nonequilibrium OAM can be generated even in the absence of spin-orbit coupling, as long as inversion symmetry is broken [12, 13]. This effect is tagged "orbital Rashba-Edelstein effect" (ORE), in analogy to the celebrated spin Rashba-Edelstein effect (SRE) that enables the electrical generation of SAM [14, 15]. Similar to SRE, ORE features an electron density that carries OAM and is limited to systems lacking inversion symmetry such as interfaces and noncentrosymmetric crystals. The OAM is not *transported* through the crystal though, but rather created *locally* which undermines its application to nonlocal orbitronics devices.

In contrast, in centrosymmetric crystals charge-neutral flows of OAM can be induced by electrical field via the orbital Hall effect [5] (OHE), the orbital analog to spin Hall effect [16] (SHE). OHE, which does not necessitate spin-orbit coupling and is only governed by the crystal field, is usually much larger than SHE [17, 18], a feature that is particularly striking in light metals [13]. Up till now, most of the effort has been focused on the transport of *intra-atomic* OAM, i.e., the angular momentum due to the gyration of the electron wave packet around the atomic nucleus only. Whereas this intra-atomic OAM is certainly an important contribution to the overall OHE, the gyration of the wave packet within the unit cell, i.e., the *inter-atomic* OAM, has been entirely overlooked [see Fig. 1(a)].

In this Letter we demonstrate that the inter-atomic OAM must be treated on equal footing as the intra-atomic OAM. We develop a theoretical framework to address both contributions, and reveal their distinct behavior in selected cases. We show that although both intra-atomic and inter-atomic contributions arise from the ground state's geometry in momentum space, the latter is much more sensitive to the details of the band structure than the former. As a result, inter-atomic OHE tends to dominate over intra-atomic OHE in the vicinity of the gap of narrow-gap semiconductors (SnTe, PbTe),

\* aurelien.manchon@univ-amu.fr

whereas intra-atomic OHE dominates in large-gap semiconductors (MoS<sub>2</sub>) as well as in transition metals (V and Pt). This distinct behavior could be exploited to design efficient orbital angular momentum sources.

**Orbital Hall conductivity** - The orbital current operator is defined  $\mathcal{J}_{o,i}^\gamma = \{\hat{v}_i, \hat{L}_\gamma\}/2$ , where  $\hat{v}$  is the velocity operator and  $\hat{\mathbf{L}} = \hat{\mathbf{r}} \times \hat{\mathbf{p}}$  is the orbital angular momentum operator in the units of the Planck constant  $\hbar$ . The indices  $i$  and  $\gamma$  denote the flow and orbital polarization directions, respectively,  $\hat{\mathbf{p}}$  is the momentum of the carrier wave packet and  $\hat{\mathbf{r}}$  represents its absolute position in the laboratory frame. In a crystal, the absolute position of the wave packet can be decomposed into three position vectors governed by completely different physical scales, as depicted on Fig. 1(b):  $\hat{\mathbf{r}} = \hat{\mathbf{r}}_u + \hat{\mathbf{r}}_a + \hat{\mathbf{r}}_c$ , where  $\hat{\mathbf{r}}_u$  refers to the position of the unit cell in the laboratory frame,  $\hat{\mathbf{r}}_a$  denotes the position of the atom on which the wave packet sits in the frame of the unit cell, and  $\hat{\mathbf{r}}_c$  is the position of this wave packet in the atom frame. These three distances embody three different length scales. In a macroscopic sample,  $|\hat{\mathbf{r}}_u| \gg |\hat{\mathbf{r}}_a|, |\hat{\mathbf{r}}_c|$  so that the OAM operator associated with it,  $\hat{\mathbf{L}}_u = \hat{\mathbf{r}}_u \times \hat{\mathbf{p}}$ , is governed by classical rather than quantum transport: it is not related to the material's band structure but rather to the macroscopic shape of the sample. In the present work, we concentrate our attention to the two other contributions, associated with the gyration of the wave packet within the unit cell,  $\hat{\mathbf{L}}_{\text{inter}} = \hat{\mathbf{r}}_a \times \hat{\mathbf{p}}$ , and around the nucleus,  $\hat{\mathbf{L}}_{\text{intra}} = \hat{\mathbf{r}}_c \times \hat{\mathbf{p}}$ . In a tight-binding approximation, one artificially separates these two contributions as the former is rather governed by processes taking place on a length scale of the order of the lattice parameter, whereas the latter is confined to the vicinity of the atom, typically over the Bohr radius.

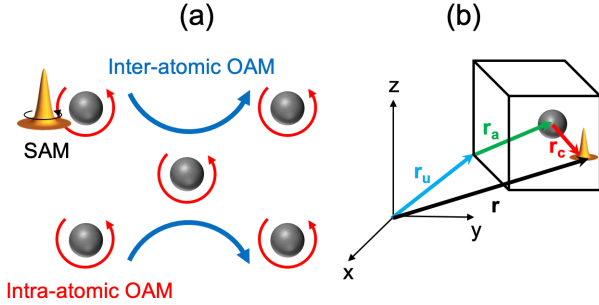


FIG. 1. (Color online) (a) Three contributions to the total angular momentum of a wave packet in a crystal: the intrinsic SAM (black arrow), the intra-atomic OAM (red arrows) and inter-atomic OAM (blue arrow). The grey spheres represent the atoms of the crystal. (b) Decomposition of the wave packet's position vector in the laboratory frame.

In the vicinity of the nucleus, the carrier wave function is better represented in a basis of spherical (or cubic) harmonics, while within the unit cell the wave packet is represented as a Bloch state that is a linear combination of the atomic orbitals composing the unit cell. In

other words, the OAM current operator can be parsed into two contributions  $\mathcal{J}_{o,i}^\gamma = \mathcal{J}_{o,i}^\gamma|_{\text{intra}} + \mathcal{J}_{o,i}^\gamma|_{\text{inter}}$ . In the linear response theory, the OAM current is time-reversal symmetric akin to the spin current, and therefore it is governed by the intrinsic Fermi sea contribution of the Kubo formula [19]. In other words, in the limit of weak momentum scattering, the OAM conductivity reads

$$\sigma_{ij}^\gamma = -e \int_{BZ} \frac{d^3\mathbf{k}}{(2\pi)^3} \sum_n f_n(\mathbf{k}) \Omega_{n,ij}^{\gamma}(\mathbf{k}), \quad (1)$$

where the orbital Berry curvature is

$$\Omega_{n,ij}^{\gamma}(\mathbf{k}) = 2\hbar \text{Im} \sum_{m \neq n} \frac{\langle u_{\mathbf{k}}^n | \mathcal{J}_{o,i}^\gamma | u_{\mathbf{k}}^m \rangle \langle u_{\mathbf{k}}^m | \hat{v}_j | u_{\mathbf{k}}^n \rangle}{(\varepsilon_{\mathbf{k}}^n - \varepsilon_{\mathbf{k}}^m)^2}. \quad (2)$$

Here,  $|u_{\mathbf{k}}^n\rangle$  is the periodic part of the Bloch state associated with the energy  $\varepsilon_{\mathbf{k}}^n$ . In addition,  $f_n(\mathbf{k})$  is the equilibrium Fermi distribution function, and  $\hat{\mathbf{v}} = \hbar^{-1} \partial_{\mathbf{k}} \mathcal{H}_{\mathbf{k}}$  is the velocity operator,  $\mathcal{H}_{\mathbf{k}}$  being the Hamiltonian in momentum space. The definition of the intra-atomic OHE,  $\mathcal{J}_{o,i}^\gamma|_{\text{intra}}$ , does not pose any difficulty because the operator  $\hat{\mathbf{L}}_{\text{intra}}$  is simply projected on spherical harmonics. In contrast, the inter-atomic contribution,  $\mathcal{J}_{o,i}^\gamma|_{\text{inter}}$ , is more subtle to determine. In the following, for the sake of clarity, we omit the subscript <sub>inter</sub>, keeping in mind that we focus on the inter-atomic OAM contribution. The interband element in Eq. (2) reads

$$\begin{aligned} \langle u_{\mathbf{k}}^n | \mathcal{J}_{o,i}^\gamma | u_{\mathbf{k}}^m \rangle &= \frac{1}{2} \sum_p \left( \langle u_{\mathbf{k}}^n | \hat{v}_i | u_{\mathbf{k}}^p \rangle \langle u_{\mathbf{k}}^p | \hat{L}_\gamma | u_{\mathbf{k}}^m \rangle \right. \\ &\quad \left. + \langle u_{\mathbf{k}}^n | \hat{L}_\gamma | u_{\mathbf{k}}^p \rangle \langle u_{\mathbf{k}}^p | \hat{v}_i | u_{\mathbf{k}}^m \rangle \right). \end{aligned} \quad (3)$$

Using the (symmetrized) definition of the OAM,  $\hat{\mathbf{L}} = (\hat{\mathbf{r}} \times \hat{\mathbf{p}} - \hat{\mathbf{p}} \times \hat{\mathbf{r}})/4$ , we obtain [20]

$$\begin{aligned} \langle u_{\mathbf{k}}^n | \hat{\mathbf{L}} | u_{\mathbf{k}}^p \rangle &= \frac{e}{2g_L \mu_B} \text{Im} \langle \partial_{\mathbf{k}} u_{\mathbf{k}}^n | \times \mathcal{H}_{\mathbf{k}} | \partial_{\mathbf{k}} u_{\mathbf{k}}^p \rangle \\ &\quad - \frac{e}{4g_L \mu_B} (\varepsilon_{\mathbf{k}}^n + \varepsilon_{\mathbf{k}}^p) \text{Im} \langle \partial_{\mathbf{k}} u_{\mathbf{k}}^n | \times | \partial_{\mathbf{k}} u_{\mathbf{k}}^p \rangle. \end{aligned} \quad (4)$$

Here,  $\mu_B = e\hbar/2m_e$  is Bohr's magneton and  $g_L = 1$  is Landé's g-factor. By considering  $|\partial_{\mathbf{k}} u_{\mathbf{k}}^n\rangle = \hbar \sum_{q \neq n} \frac{\langle u_{\mathbf{k}}^q | \hat{\mathbf{v}} | u_{\mathbf{k}}^n \rangle}{\varepsilon_{\mathbf{k}}^q - \varepsilon_{\mathbf{k}}^n} |u_{\mathbf{k}}^q\rangle$ , we finally deduce that

$$\begin{aligned} \langle u_{\mathbf{k}}^n | \hat{\mathbf{L}} | u_{\mathbf{k}}^p \rangle &= \frac{e\hbar^2}{4\mu_B} \text{Im} \sum_{q \neq n,p} \left( \frac{1}{\varepsilon_{\mathbf{k}}^q - \varepsilon_{\mathbf{k}}^n} + \frac{1}{\varepsilon_{\mathbf{k}}^q - \varepsilon_{\mathbf{k}}^p} \right) \\ &\quad \langle u_{\mathbf{k}}^n | \hat{\mathbf{v}} | u_{\mathbf{k}}^q \rangle \times \langle u_{\mathbf{k}}^q | \hat{\mathbf{v}} | u_{\mathbf{k}}^p \rangle. \end{aligned} \quad (5)$$

Inserting Eq. (5) into Eq. (3), we infer the expression of the inter-atomic OHE. It is important to emphasize a key difference between the intra-atomic and inter-atomic Hall transports. Whereas both effects are inversely proportional to  $(\varepsilon_{\mathbf{k}}^n - \varepsilon_{\mathbf{k}}^m)^2$  [Eq. (2)], suggesting hot spots close to avoided band crossing in the Brillouin zone, the inter-atomic orbital current is additionally influenced by a factor proportional to the relative energy difference between bands,  $\varepsilon_{\mathbf{k}}^n - \varepsilon_{\mathbf{k}}^m$  [Eq. (5)]. Therefore, we expect

the inter-atomic OHE to be more sensitive to the band ordering than the intra-atomic OHE, which could lead to cancellation when numerous bands are involved (e.g., in a transition metal). We now evaluate these two contributions in selected examples.

*Minimal model for OHE* - To evaluate the impact of the aforementioned OHE contributions, we first select a minimal model with a restricted set of spinless atomic orbitals (typically,  $p_x$  and  $p_y$ ). An example of such a toy model was introduced by Fu [21] as a paradigm for topological crystalline insulators. From our standpoint, this model presents the advantage that its topological properties are due to its orbital chirality rather than its spin chirality. It consists of a square bipartite lattice whose Hamiltonian reads

$$\mathcal{H} = \sum_n \mathcal{H}_n^A + \mathcal{H}_n^B + \mathcal{H}_n^{AB}, \quad (6)$$

where the Hamiltonian for each sublattice  $\mathcal{H}_n^a$ ,  $a = A, B$ , and the coupling Hamiltonian  $\mathcal{H}_n^{AB}$  are given by

$$\begin{aligned} \mathcal{H}_n^a &= \sum_{i,j} t^a(\mathbf{r}_i - \mathbf{r}_j) \sum_{\alpha,\beta} c_{a,\alpha}^\dagger(\mathbf{r}_i, n) e_{\alpha}^{i,j} e_{\beta}^{i,j} c_{a,\beta}(\mathbf{r}_j, n), \quad (7) \\ \mathcal{H}_n^{AB} &= \sum_{i,j} t'(\mathbf{r}_i - \mathbf{r}_j) \left[ \sum_{\alpha} c_{A,\alpha}^\dagger(\mathbf{r}_i, n) c_{B,\alpha}(\mathbf{r}_j, n) + h.c. \right] \\ &\quad + t'_z \sum_i \sum_{\alpha} [c_{A,\alpha}^\dagger(\mathbf{r}_i, n) c_{B,\alpha}(\mathbf{r}_i, n+1) + h.c.]. \quad (8) \end{aligned}$$

Each site is identified by the bilayer unit cell  $n$ , the planar coordinate in each layer  $\mathbf{r} = (x, y)$  and the sublattice label  $a = A, B$ . Since in Eq.(6) we have two orbitals per site, these are represented by the indices  $\alpha$  or  $\beta$ . The hopping terms display a direction given by the unit vectors  $e^{i,j} = (\mathbf{r}_i - \mathbf{r}_j)/|\mathbf{r}_i - \mathbf{r}_j|$ . This model preserves the crystal symmetries for the Hamiltonian. Besides, we recall that this setup can represent a  $p_{x,y}$  system just like a  $d_{xz,yz}$  one since both transform in the same way under  $C_4$ .

In Fig. 2, we show both intra-atomic and inter-atomic contributions to the orbital Hall conductivity  $\sigma_{xy}^z$  computed using Eq. (1). Let us first focus on the behavior of the OHE in the gap. As mentioned above, the model features a topological crystalline insulator that supports topological surface states [21]. We find that in the gap, these surface states do not carry intra-atomic OHE, but do carry a finite inter-atomic OHE [Fig. 2(a)], an aspect that was overlooked in Ref. [21]. Remarkably, when projected on each sublattice, the intra-atomic OHE is quantized and staggered [red and green lines in Fig. 2(b)]. In other words, Fu's model does not realize quantum orbital Hall insulator, but rather a quantum 'staggered' orbital Hall insulator. Conversely, the inter-atomic OHE does not vanish and gives a constant (but not quantized) value in the gap, as shown in Fig. 2(a). Notice that due to the inter-atomic nature of this contribution, it cannot be projected on each sublattice. We attribute this behaviour to the Berry curvature appearing near the 'A' point, as

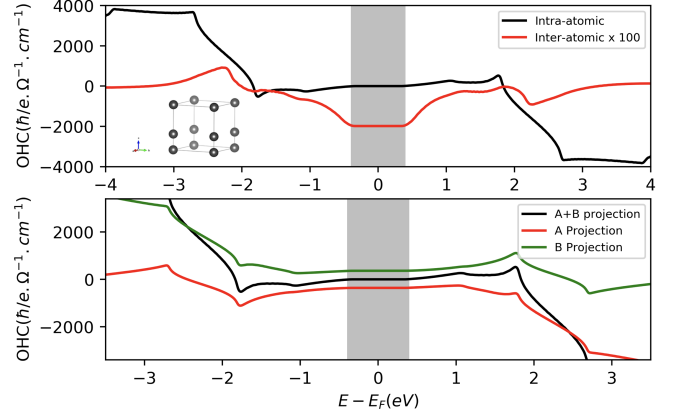


FIG. 2. (Color online) (a) Orbital Hall conductivity computed for the 4-band model. We compute both intra-atomic (black) and inter-atomic (red) contributions. (b) Intra-atomic orbital Hall response projected on sublattices A (green) and B (blue). These projections give equal and opposite values of the Hall response in the gap, leading to a vanishing total intra-atomic contribution. The parameters are set to  $t_1^a = -t_1^b = 1$ ,  $t_2^a = t_2^b = 0.5$ ,  $t_1' = 2.5$ ,  $t_2' = 0.5$ ,  $t_z = 2$ . The inset displays the unit cell.

depicted in the Supplementary Material [20]. Another important point is that whereas inter-atomic OHE dominates in the gap, intra-atomic OHE dominates away from the gap. This observation points out that both intra-atomic and inter-atomic contributions must be in fact taken into account when computing the OHE in multi-band systems.

*Realistic material simulations* - We now turn to the simulation of OHE in real materials. We start by considering well-known semiconductors that display strong orbital hybridization in their band structure. As paradigmatic narrow-gap semiconductors, we select the three-dimensional topological crystalline insulator SnTe [22], and its topologically trivial parent compound, PbTe, both of which possess large  $p$  orbitals hybridization near the gap located at the L points in the Brillouin zone. As an example of large-gap semiconductor, we chose MoS<sub>2</sub>-2H monolayer. In fact, MoS<sub>2</sub> and transition metal dichalcogenide siblings possess two valleys at K and K' points in the Brillouin zone and support valley Hall effect [23]. We perform density functional theory (DFT) simulations [24, 25] using the Perdew-Burke-Ernzerhof [26, 27] exchange-correlation functional. We achieved the geometry optimizations with the plane-wave basis as implemented in the Vienna *Ab-initio* Simulation Package (VASP) [28, 29]. For SnTe and PbTe, we used a 400 eV cutoff for the plane-wave expansion along with a force criterion  $< 5 \mu\text{eV}/\text{\AA}$  with a  $15 \times 15 \times 15$   $\mathbf{k}$ -points sampling of the Brillouin zone. The ionic potentials were described using the projector augmented-wave (PAW) method [30]. For MoS<sub>2</sub>-2H monolayer, we used a 350 eV cutoff with  $15 \times 15 \times 1$  Monkhorst pack for the  $\mathbf{k}$ -grid. Taking a 15Å vacuum to avoid interaction with mirror

images, the structure was relaxed such that the forces satisfied the criterion  $< 10 \mu\text{eV}/\text{\AA}$ .

In all three cases, the Hamiltonian matrix was obtained by Wannier interpolation as implemented in the Wannier90 package [31]. For SnTe and PbTe, we have used the  $s$  and  $p$  orbitals which are responsible for the electronic properties of this material around the  $L$  high symmetry point [32, 33], whereas for MoS<sub>2</sub>-2H monolayer we have used a basis considering the transition metal  $d$  orbitals along with the chalcogen  $p$  orbitals. Finally, in each case we have symmetrized the real space Hamiltonian by imposing lattice symmetry constraints [34]. The bands structures are displayed in [20].

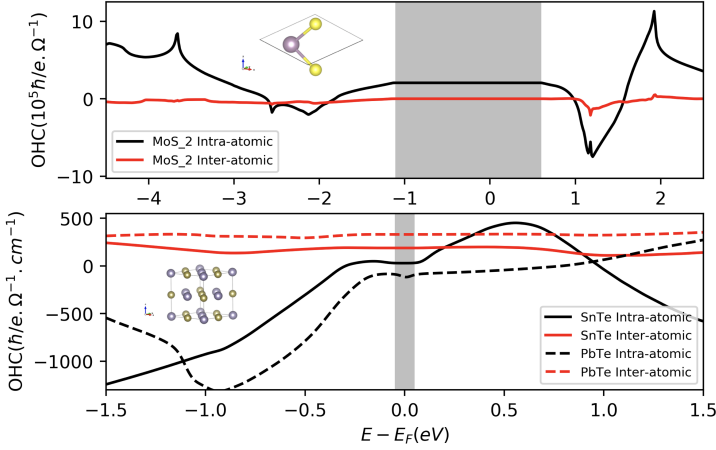


FIG. 3. (Color online) Intra-atomic and inter-atomic orbital contributions to the OHE for (a) MoS<sub>2</sub>-2H, and (b) SnTe, PbTe where both intra-atomic (black lines) and inter-atomic (red lines) contributions are depicted. The inset displays the unit cell for each case.

The intra-atomic and inter-atomic orbital Hall conductivities are reported in Fig. 3 for (a) MoS<sub>2</sub>, as well as for (b) SnTe and PbTe. In MoS<sub>2</sub>, since each valley is associated with an OAM of opposite sign, one should expect that the valley Hall effect is accompanied by an OHE, as pointed out recently [35–37]. We emphasize that all these previous works focus on the intra-atomic OHE, disregarding the inter-atomic counterpart. In fact, in agreement with these studies, we obtain a finite value of the intra-atomic OHE in the gap for MoS<sub>2</sub> (black line), whereas the inter-atomic OHE vanishes (red line). This finite, but not quantized, value of the intra-atomic OHE in the gap reveals that the edge states lack robustness when disorder is included [38].

The narrow-gap semiconductors, SnTe and PbTe, offer a strikingly different picture, see Fig. 3(b). SnTe has an inverted gap of  $\sim 0.15$  eV and the active region near the gap is mostly composed of  $p$  orbitals. The same is true for PbTe although with a narrower gap ( $\sim 0.08$  eV) and no band inversion. We find that the inter-atomic OHE (red lines) is larger than the intra-atomic one (black lines) in the vicinity of the gap, irrespective of the topological nature of the band structure. In the case of SnTe, the intra-

atomic OHE vanishes in the gap, whereas for PbTe, it is finite. Most importantly, in both cases, the intra-atomic OHE dominates away from the gap, confirming the qualitative picture obtained in the minimal model presented above. Remarkably, we notice that the magnitude of the inter-atomic OHE scales inversely with the gap: it decreases from PbTe to SnTe and vanishes in MoS<sub>2</sub>, which can be understood from Eq. 5: the large gap present near the valley points quenches the inter-atomic OAM. The inter-atomic OAM is therefore a substantial contribution to OHE in narrow-gap semiconductors.

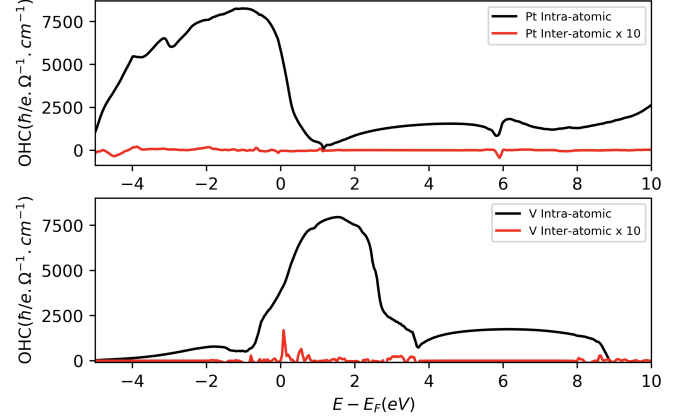


FIG. 4. (Color online) Intra-atomic and inter-atomic contributions to the OHE for (a) Pt and (b) V. Both intra-atomic (black lines) and inter-atomic (red lines) contributions are depicted.

In the systems discussed so far, we have considered semiconductors whose band structure in the vicinity of the gap is reasonably modelled by a few bands only. We now move on to transition metals that display no gap and involve a large number of bands close to Fermi level. In Fig. 4, we show the intra-atomic and inter-atomic OHE for two representative metallic materials with large [Pt, Fig. 4(a)] and weak spin-orbit coupling [V, Fig. 4(b)]. The large values we obtain for the intra-atomic OHE are in good agreement with those documents in the literature [13], exceeding by a large margin those of the inter-atomic OHE. We attribute the quenching of the inter-atomic OHE to the multiband nature of the transition metals' band structure. Indeed, since the inter-atomic OHE is sensitive to the *relative* energy difference between bands, the presence of a large number of bands at Fermi level favors the overall cancellation of the inter-atomic OAM in metals.

*Discussion and conclusion* - We have demonstrated that the OHE arises from both intra-atomic and inter-atomic effects, associated with the electron wave packet gyration around the atomic nucleus and inside the unit cell, respectively. In principle, both contributions should be accounted for when evaluating OHE in real materials. Nonetheless, these two contributions present drastic differences: the inter-atomic part is more sensitive to band ordering and local energy gaps than the intra-atomic one.

Investigating these effects on different classes of materials, we propose the following guiding rules. Our results suggest that the intra-atomic contribution tends to dominate over the inter-atomic one away from the gap, irrespective of the materials' band structure details. This is particularly meaningful for metals, where intra-atomic OHE largely dominates. Nonetheless, in semiconductors the situation is very sensitive to the magnitude of the gap: while the intra-atomic OHE dominates in large gap semiconductors, the inter-atomic contribution becomes sizable in narrow-gap semiconductors, and even dominant close to the gap. In the race to identify efficient sources of orbital currents, these observations point out that two-dimensional semiconductors could be particularly promising candidates.

Finally, we found that OHE might show finite value in the gap, even in the absence of topological surface or edge states, raising the question of their topological fragility against perturbation. This is a seminal question for the

design of orbitronic devices, which do not only rely on the ability to generate orbital currents but also on the robustness of these currents against disorder and injection through interfaces. From the derivation described in this Letter, we are inclined to speculate that intra-atomic and inter-atomic contributions might not present the same robustness against disorder, due to the high sensitivity of the latter to band ordering.

## ACKNOWLEDGMENTS

This work was supported by the ANR ORION project, grant ANR-20-CE30-0022-01 of the French Agence Nationale de la Recherche. D. G.O. and A. M. acknowledge support from the Excellence Initiative of Aix-Marseille Université - A\*Midex, a French "Investissements d'Avenir" program. The authors thank A. Saul for numerous fruitful discussions.

- 
- [1] E. Y. Vedmedenko, R. K. Kawakami, D. D. Sheka, P. Gambardella, A. Kirilyuk, A. Hirohata, C. Binek, O. Chubykalo-Fesenko, S. Sanvito, B. J. Kirby, J. Grollier, K. Everschor-Sitte, T. Kampfrath, C. Y. You, and A. Berger, *Journal of Physics D: Applied Physics* **53**, 453001 (2020).
  - [2] A. V. Chumak, V. I. Vasyuchka, A. A. Serga, and B. Hillebrands, *Nature Physics* **11**, 453 (2015).
  - [3] S. A. Vitale, D. Nezich, J. O. Varghese, P. Kim, N. Gedik, P. Jarillo-herrero, D. Xiao, and M. Rothschild, *Small* **14**, 1801483 (2018).
  - [4] A. Manchon, J. Zelezný, M. Miron, T. Jungwirth, J. Sinova, A. Thiaville, K. Garello, and P. Gambardella, *Review of Modern Physics* **91**, 035004 (2019).
  - [5] B. A. Bernevig, T. L. Hughes, and S.-c. Zhang, *Physical Review Letters* **95**, 066601 (2005).
  - [6] D. Go, D. Jo, C. Kim, and H. W. Lee, *Physical Review Letters* **121**, 086602 (2018).
  - [7] T. Thonhauser, D. Ceresoli, D. Vanderbilt, and R. Resta, *Physical Review Letters* **95**, 137205 (2005), arXiv:0505518 [cond-mat].
  - [8] D. Ceresoli, T. Thonhauser, D. Vanderbilt, and R. Resta, *Physical Review B* **74**, 024408 (2006), arXiv:0512142 [cond-mat].
  - [9] J. Shi, G. Vignale, D. Xiao, and Q. Niu, *Physical Review Letters* **99**, 197202 (2007).
  - [10] J. Hanke, F. Freimuth, A. K. Nandy, H. Zhang, S. Bl, Y. Mokrousov, and P. Gr, *Physical Review B* **94**, 121114(R) (2016).
  - [11] J.-p. Hanke, F. Freimuth, S. Blügel, and Y. Mokrousov, *Scientific Reports* **7**, 41078 (2017).
  - [12] T. Yoda, T. Yokoyama, and S. Murakami, *Nano Letters* **18**, 916 (2018).
  - [13] D. Jo, D. Go, and H.-w. Lee, *Physical Review B* **98**, 214405 (2018).
  - [14] V. M. Edelstein, *Solid State Communications* **73**, 233 (1990).
  - [15] A. Manchon, H. C. Koo, J. Nitta, S. M. Frolov, and R. A. Duine, unpublished (2015).
  - [16] J. Sinova, S. O. Valenzuela, J. Wunderlich, C. H. Back, and T. Jungwirth, *Review of Modern Physics* **87**, 1213 (2015).
  - [17] T. Tanaka, H. Kontani, M. Naito, T. Naito, D. Hirashima, K. Yamada, and J. Inoue, *Physical Review B* **77**, 165117 (2008).
  - [18] H. Kontani, T. Tanaka, D. Hirashima, K. Yamada, and J. Inoue, *Phys. Rev. Lett.* **100**, 096601 (2008).
  - [19] V. Bonbien and A. Manchon, *Physical Review B* **102**, 085113 (2020).
  - [20] "Supplemental Materials,".
  - [21] L. Fu, *Physical Review Letters* **106**, 106802 (2011).
  - [22] T. H. Hsieh, H. Lin, J. Liu, W. Duan, A. Bansil, and L. Fu, *Nature communications* **3**, 982 (2012), arXiv:1202.1003.
  - [23] D. Xiao, G.-B. Liu, W. Feng, X. Xu, and W. Yao, *Physical Review Letters* **108**, 196802 (2012).
  - [24] P. Hohenberg and W. Kohn, *Phys. Rev.* **136**, B864 (1964).
  - [25] W. Kohn and L. J. Sham, *Phys. Rev.* **140**, A1133 (1965).
  - [26] J. P. Perdew, J. A. Chevary, S. H. Vosko, K. A. Jackson, M. R. Pederson, D. J. Singh, and C. Fiolhais, *Phys. Rev. B* **46**, 6671 (1992).
  - [27] J. P. Perdew, K. Burke, and M. Ernzerhof, *Physical Review Letters* **77**, 3865 (1996), arXiv:0927-0256(96)00008 [10.1016].
  - [28] G. Kresse and J. Furthmüller, *Computational Materials Science* **6**, 15 (1996).
  - [29] G. Kresse and J. Furthmüller, *Physical Review B* **54**, 11169 (1996).
  - [30] G. Kresse and D. Joubert, *Physical Review B* **59**, 1758 (1999).
  - [31] G. Pizzi, V. Vitale, R. Arita, S. Blügel, F. Freimuth, G. Géranton, M. Gibertini, D. Gresch, C. Johnson, T. Koretsune, J. Ibanez-Azpiroz, H. Lee, J. M. Lihm, D. Marchand, A. Marrazzo, Y. Mokrousov, J. I. Mustafa,

- Y. Nohara, Y. Nomura, L. Paulatto, S. Poncé, T. Ponweiser, J. Qiao, F. Thöle, S. S. Tsirkin, M. Wierzbowska, N. Marzari, D. Vanderbilt, I. Souza, A. A. Mostofi, and J. R. Yates, *Journal of Physics Condensed Matter* **32**, 165902 (2020), arXiv:1907.09788.
- [32] Z. Y. Ye, H. X. Deng, H. Z. Wu, S. S. Li, S. H. Wei, and J. W. Luo, *npj Computational Materials* **1**, 15001 (2015).
- [33] P. B. Littlewood, B. Mihaila, R. K. Schulze, D. J. Sarik, J. E. Gubernatis, A. Bostwick, E. Rotenberg, C. P. Opeil, T. Durakiewicz, J. L. Smith, and J. C. Lashley, *Physical Review Letters* **105**, 086404 (2010), arXiv:1008.4148.
- [34] G.-X. Zhi, C. Xu, S.-Q. Wu, F. Ning, and C. Cao, *Computer Physics Communications* **271**, 108196 (2022), arXiv:2110.11764.
- [35] S. Bhowal and S. Satpathy, *Phys. Rev. B* **101**, 121112 (2020).
- [36] L. M. Canonico, T. P. Cysne, A. Molina-Sanchez, R. B. Muniz, and T. G. Rappoport, *Phys. Rev. B* **101**, 161409 (2020).
- [37] T. P. Cysne, M. Costa, L. M. Canonico, M. B. Nardelli, R. B. Muniz, and T. G. Rappoport, *Phys. Rev. Lett.* **126**, 056601 (2021).
- [38] A. Pezo, M. P. Lima, M. Costa, and A. Fazzio, *Phys. Chem. Chem. Phys.* **21**, 11359 (2019).